

# New Solar Models Including Helioseismological Constraints and Light-Element Depletion

O. Richard<sup>1</sup>, S. Vauclair<sup>1</sup>, C. Charbonnel<sup>1</sup>, and W.A. Dziembowski<sup>2</sup>

<sup>1</sup> Observatoire Midi-Pyrénées 14, avenue Edouard Belin, 31400 Toulouse, France

<sup>2</sup> Copernicus Astronomical Center, Warsaw, Poland

Received ; accepted

**Abstract.** We have computed new solar models using the same stellar evolution code as described in Charbonnel, Vauclair and Zahn (1992). This code, originating from Geneva, now includes the computation of element segregation for helium and 12 heavier isotopes. It may also include any type of mixing of the stellar gas, provided this mixing can be parametrized with an effective diffusion coefficient as a function of radius. Here we introduced rotation-induced mixing as prescribed by Zahn (1992). We present five solar models: 1) the standard model, computed with heavy element abundances as given by Grevesse (1991); 2) a model including pure element segregation (no mixing outside the convective zone) with Grevesse (1991) as initial abundances; 3) same model as (2), but iterated so that the final abundances are those of Grevesse (1991); 4) a model with both element segregation and rotation-induced mixing, leading to lithium and beryllium depletion consistent with the observations, with Grevesse (1991) as initial abundances; 5) same model as (4) but iterated to obtain Grevesse (1991) as final abundances. This model (5) now represents our best new solar model consistent with the observations.

The  $u = \frac{P}{\rho}$  function computed as a function of radius in these new solar models are compared to the helioseismological results obtained for the same function by Dziembowski et al (1994). Improving the physics of the models leads to a better consistency with helioseismology. In our best model (5), which includes both segregation and mixing, the relative difference in the  $u$  function between the model and the helioseismological results is smaller than 0.5 per cent at all radii except at the center and the surface. Meanwhile lithium is depleted by a factor 155 and beryllium by a factor 2.9, which is consistent with the observations. The bottom of the convective zone lies at a fractional radius of 0.716, consistent with helioseismology. The neutrino fluxes are not decreased in any of these models.

The models including the computations of element segregation lead to a present surface helium abundance of:  $Y_{surf}$  between 0.248 and 0.258, which is in satisfactory agreement with the value derived from helioseismology.

**Key words:** Physical data and processes : diffusion – Sun : abundances - evolution - interior - rotation

## 1. Introduction

The Sun is by far the most well known of all the stars. Its mass, radius, luminosity and age have been determined with a high degree of precision (Table 1). The mass is obtained from the motion of planets, the radius from eclipses (the value given in table 1 is reduced to an optical depth  $\tau=2/3$ ), the luminosity from measurements of the solar constant above the earth's atmosphere. Some discussion remains about the solar age: it is generally taken as 4.6 billion years although Guenther (1989) and Demarque and Guenther (1991) suggest a smaller age consistent with the oldest meteorites. The photospheric solar element abun-

**Table 1.** Solar parameters

mass	$(1.9891 \pm 0.0004) \times 10^{33}$ g
radius	$(6.959 \pm 0.001) \times 10^{10}$ cm
luminosity	$(3.851 \pm 0.005) \times 10^{33}$ ergs.s <sup>-1</sup>
age	$4.6 \pm 0.15$ Gyr
mass loss	$2 \times 10^{-14}$ M <sub>⊙</sub> .yr <sup>-1</sup>

dances are now precisely known, after the studies by Anders and Grevesse (1989) modified by Grevesse (1991). See also Grevesse and Anders (1991). Lithium and beryllium are both depleted in the Sun with ratios :

$$Li/Li_o = 1/140 \quad ; \quad Be/Be_o = 1/2$$

with an relative uncertainty of 30% in both cases. Any consistent solar model must account for these depletion factors.

The study of the internal structure of the Sun entered a new age with the birth of helioseismology. Millions of solar p-modes have been detected (including the  $(2l + 1)$  multiplets). An inversion of the measured frequencies yields accurate and detailed information about such structural functions as pressure,  $p(r)$ , and density,  $\rho(r)$ , in the Sun's interior. A particularly high precision is achieved in the determination of  $u = \frac{p}{\rho}$  throughout the Sun, and in the localization of the bottom of the convective envelope. No assumption regarding the transport of energy and chemical elements is introduced at this stage of seismic sounding. The only essential assumption is that of mechanical equilibrium, which is partially testable by means of helioseismology.

Christensen-Dalsgaard et al. (1993) have shown that gravitational settling and element mixing processes significantly affect the calculated speed of sound near the bottom of the convective envelope. These processes lead to a lower surface helium abundance - a quantity which may also be directly inferred from helioseismic data if the equation of state is specified. The results of many independent inversions clearly demonstrate that helium settling must take place in the Sun. A question we ask in this paper is whether helioseismology provides useful constraints on the mixing processes.

An important result of helioseismology is the precise determination of the bottom of the solar convective zone:  $\frac{r_{cz}}{R_{\odot}} = 0.713 \pm 0.003$  (Christensen- Daalsgard et al. 1993). This value corresponds to that obtained from the Schwarzschild criterium, leading to a strong constraint on overshooting (section 3). In the following we show that, contrary to a common idea generally spread among solar physicists, this constraint on overshooting is not a problem for the explanation of the lithium depletion in the Sun. In any case, explaining the lithium depletion in the Sun by overshooting would not be consistent with the lithium observations in other stars (e.g. galactic clusters).

Charbonnel, Vauclair and Zahn (1992) (CVZ) and Charbonnel et al. (1994) showed that the lithium deficiency in solar type stars can be accounted for by rotation-induced mixing. We will show here that such a mixing can also account for Li and Be depletion in the Sun, without destroying the consistency with helioseismology.

The recipe to construct solar models is well known and has been explained many times in the literature (Cox, Guzik and Kidman 1989, Bahcall and Pinsonneault 1992, Turck-Chieze and Lopes 1993, Proffitt 1994 etc.). We begin with a homogeneous  $1M_{\odot}$  model on the zero-age main sequence. Then the model is evolved step by step, by taking into account the modification of the chemical composition due to nuclear reactions. At the age of the Sun, it must reproduce the data given in table 1 within the observed uncertainties. To obtain such a high precision,

two parameters are traditionally adjusted, with an iteration procedure: the  $^4\text{He}$  mass fraction  $Y$  and the ratio of the convective mixing length to the pressure scale height, generally referred to as  $\alpha$ .

The computation of the standard solar models includes the assumption that the stellar gas as a whole is in hydrostatic equilibrium. This fundamental "first equation" of the internal structure of stars assumes that a blob of stellar gas is in equilibrium due to the effect of gravity downwards and pressure gradient upwards, which is correct in first approximation. It does not take however into account the fact that the stellar gas is a mixture of many different species, which do not have the same weight. This is the problem of element segregation, which indeed is a fundamental process inherent to the stellar structure.

In this paper we present new solar models computed with a stellar evolution code including element segregation and mixing, as described in CVZ. The physics included in these computations is discussed in section 2, a discussion about helioseismology appears in section 3 and the results are given in section 4.

Five solar models will be discussed: 1) the best standard model 2) a model including pure element segregation (no mixing outside the convective zone) with initial abundances corresponding to the Grevesse (1991) mixture; 3) same model as (2), but iterated so that the final abundances are those of Grevesse (1991); 4) a model with both element segregation and rotation-induced mixing, leading to lithium and beryllium depletion consistent with the observations, with Grevesse (1991) as initial abundances; 5) same model as (4) but iterated to obtain Grevesse (1991) as final abundances. This model (5) now represents our best new solar model consistent with the observations.

All these models are compared to the helioseismological results obtained by Dziembowski et al (1994). It is very encouraging to see that improving the physics of the models leads to a very good consistency with helioseismology. In our best model (5), which includes both segregation and mixing, the relative difference in the  $u$  function between the model and the helioseismological results is smaller than 0.5 per cent at all radii except at the center and the surface. Meanwhile lithium is depleted by a factor 150 and beryllium by a factor 2.9, which is consistent with the observations. The bottom of the convective zone lies at a fractional radius of 0.716, consistent with helioseismology.

The computed neutrino fluxes will be presented in the tables of results for each models. They are not decreased in any of them. These results will be shortly discussed but a complete discussion of the solar neutrino problem is out of the scope of the present paper.

**Table 2.** Initial parameter and main physical surface parameter of solar models.

	$Y_0$	$\alpha$	$Y_{surface}$	$X_{surface}$	L ( $10^{34}\text{erg.s}^{-1}$ )	R ( $10^{11}\text{cm}$ )	Li/Li <sub>0</sub>	Be/Be <sub>0</sub>
Model 1	0.2782	1.652	0.2782	0.7028	0.385145	0.695976	1	1
Model 2	0.2762	1.776	0.2477	0.7341	0.385154	0.696368	1/2.89	1/1.17
Model 3	0.2798	1.789	0.2513	0.7297	0.385143	0.695982	1/3.50	1/1.17
Model 4	0.2770	1.761	0.2563	0.7252	0.385131	0.695980	1/124.58	1/2.88
Model 5	0.2793	1.768	0.2584	0.7226	0.384993	0.695849	1/155.03	1/2.91

**Table 3.** Main physical parameter of solar models at the base of the convective zone and at the center.

	$\frac{r_{cz}}{R_{\odot}}$	$T_{cz}$ ( $10^6\text{K}$ )	$\rho_{cz}$ ( $\text{g.cm}^{-3}$ )	$Y_c$	$X_c$	$T_c$ ( $10^6\text{K}$ )	$\rho_c$ ( $\text{g.cm}^{-3}$ )	$P_c$ ( $\text{dyn.cm}^{-2}$ )
Model 1	0.725	2.100	0.166	0.6346	0.3459	15.56	150.66	$2.303 \cdot 10^{17}$
Model 2	0.716	2.158	0.185	0.6416	0.3383	15.63	153.81	$2.344 \cdot 10^{17}$
Model 3	0.714	2.178	0.189	0.6464	0.3326	15.70	154.17	$2.345 \cdot 10^{17}$
Model 4	0.717	2.162	0.185	0.6431	0.3368	15.63	154.17	$2.350 \cdot 10^{17}$
Model 5	0.716	2.175	0.188	0.6465	0.3328	15.67	154.53	$2.350 \cdot 10^{17}$

## 2. The computations

### 2.1. Input microphysics

– Equation of state : The present solar models are computed with the equation of state developed by Hummer & Mihalas (1988), Mihalas et al. (1988), Däppen et al. (1988), hereafter MHD. The MHD equation of state is based on the free-energy minimization method which implies that it is thermodynamically consistent. It treats pressure ionization carefully and takes into account non ideal effects such as Coulomb correction to pressure, pressure due to partially degenerate electrons and correction for size of particles. It also includes a large number of atomic, ionic and molecular species, with detailed partition functions, containing weighted occupation probabilities. As shown by Christensen-Dalsgaard et al. (1988), the MHD equation of state highly improves the solar models in the helioseismological context.

– Opacities : We use the OPAL radiative opacities by Iglesias et al. (1992) which include the spin-orbit interactions for Fe and relative metal abundances based on Grevesse (1991). These tables are complemented at low temperatures below 10000K with the atomic and molecular opacities by Kurucz (1991).

– Nuclear reactions : For hydrogen-burning we consider the tree pp chains and the CNO tri-cycle. We use the thermonuclear reaction rates Caughlan & Fowler (1988). Screening factors for the reaction rates are taken into account according to the analytical prescription by Graboske et al. (1973).

The key reaction for the generation of high energy neutrinos and for the theoretical neutrino flux to be compared to the chlorine experiments results is  ${}^7\text{Be}(p,\gamma){}^8\text{B}$ . Caughlan & Fowler (1988) give a value of 0.0240 keV-barns for the corresponding low energy cross section factor,  $S_{17}(0)$ , which is extrapolated from experimentally measured reaction cross sections.

### 2.2. Element Segregation

The process of element segregation in stars (also referred to as “microscopic diffusion”) represents a basic physical process inherent to the stellar structure. As soon as the stars form out of gas clouds, they built density, pressure and temperature gradients throughout. Under such conditions, the various chemical species present in the stellar gas move with respect to one another, unless macroscopic motions force the chemical homogeneization.

Although recognized by the pioneers of the study of stellar structure (Eddington, 1916 and 1926, Chapman, 1917), this process was long forgotten in the computations of stellar models, except for white dwarfs (Schatzman, 1945). Only with the discovery of large abundance anomalies in main-sequence type stars (the so-called Ap and Am stars), which present characteristic variations of chemical elements with the effective temperature, was microscopic diffusion brought into light fifty years later (Michaud, 1970, see other references in Vauclair and Vauclair, 1982).

At that time, the effects of microscopic diffusion were supposed to be important only when the diffusion time scale was smaller than the stellar age. In the Vauclair and

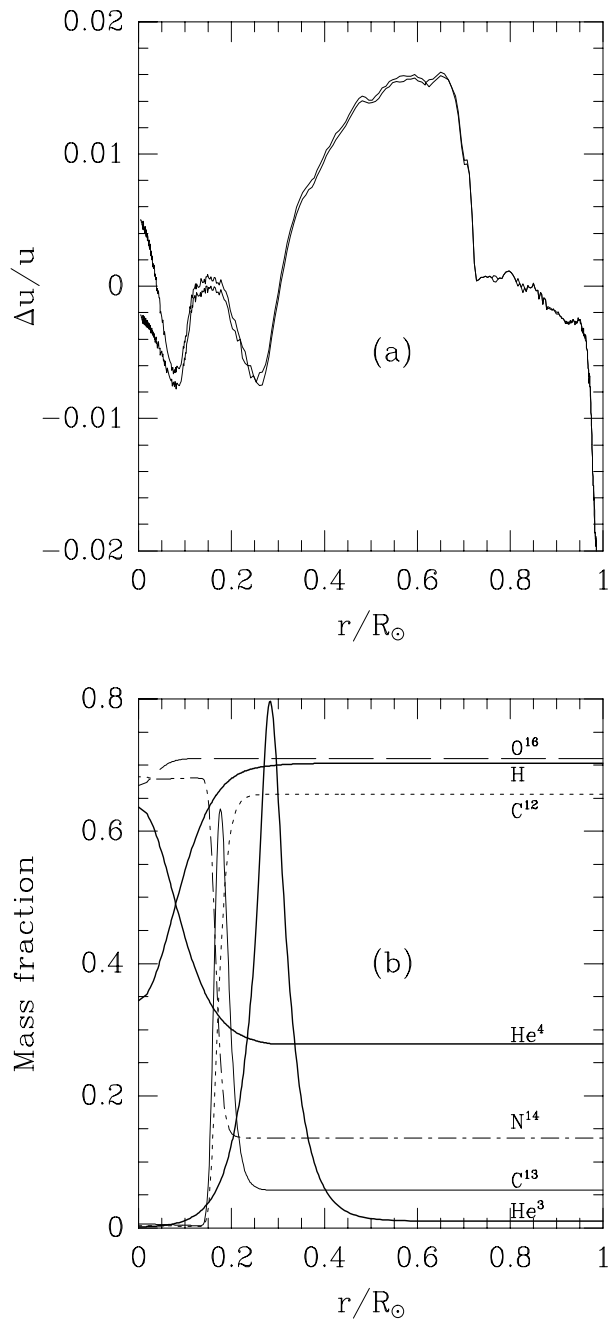


**Fig. 1.** Standard Solar model (model 1). The top graph represents the difference between the  $u$  function ( $u = \frac{P}{\rho}$ ) deduced from helioseismology and the computed one. The ordinates represents :  $\frac{\Delta u}{u} = \frac{u(\text{seismic}) - u(\text{model})}{u(\text{seismic})}$

The bottom graph shows the abundance profiles for some elements in the two models (The mass fractions are multiplied by 250 for  $^3\text{He}$ , by 200 for  $^{12}\text{C}$ , by 1000 for  $^{13}\text{C}$ , by 140 for  $^{14}\text{N}$  and by 75 for  $^{16}\text{O}$ ).

Vauclair (1982) review paper, Fig. 1 shows the regions in the HR diagram where microscopic diffusion could lead to “observable” abundance variations. The Sun was excluded, although at the border of the “permitted domain”. In the present days, due to helioseismology, abundance variations of the order of a few percent become indirectly detectable: we have entered a new area in this respect.

Several authors have computed the gravitational and thermal diffusion of helium and heavier elements in the Sun with various approximations (see references in Michaud and Vauclair, 1991). More recently the influence of diffusion on the solar oscillation modes and on the solar neutrino fluxes have been studied in various ways (Cox, Guzik, Kidman, 1989; Bahcall and Pinsonneault, 1992; Proffitt, 1994; Thoul, Bahcall and Loeb, 1994).

Element segregation represents in fact a competition between two kinds of processes. First the atoms move under the influence of external forces (due to gravity, radiation, etc.), second they collide with other atoms and share the acquired momentum with them in a random way, which slows down their motion. This competition leads to element stratification and decreases the entropy.

The computations of microscopic diffusion are based on the Boltzmann equation for dilute collision-dominated plasmas. At equilibrium the solution of the equation is the maxwellian distribution function:  $f = f(0)$ . In stars the distribution is not maxwellian, but the deviations from the maxwellian distribution are very small. Two different methods are developed to solve the Boltzmann equation in this framework. The first method relies on the Chapman-Enskog procedure (described in Chapman and Cowling, 1970), with convergent series of  $f$  computed with successive approximations. This method is used, for example, by Bahcall and Loeb (1990), Proffitt and Michaud (1991), Michaud and Vauclair (1991), Bahcall and Pinsonneault (1992) and CVZ, in which a complete description of the numerical schemes may be found.

The second method is that of Burgers (1969), in which separate flow and heat equations for each component of a multi-component mixture are solved simultaneously. Descriptions of this method may be found for example in Cox, Guzik and Kidman (1989), Proffitt and Vandenberg (1991), Thoul, Bahcall and Loeb (1994), Richer and Michaud (1993). This method does not include for the moment the problem of partial ionisation which has been studied within the framework of the Chapman and Cowling method (Montmerle and Michaud 1976; Vauclair, Hardorp, Peterson, 1979; Alecian and Vauclair, 1981).

In the present paper the first method has been used for the treatment of the Boltzmann equation, as described in CVZ. For collisions between charged ions, the Paquette et al. (1986) method has been introduced. The basic question concerns the divergence of the coulomb interaction cross sections. In the first computations of diffusion, the “Chapman and Cowling approximation” was used, assuming a cut-off of the cross section equal to the Debye shielding

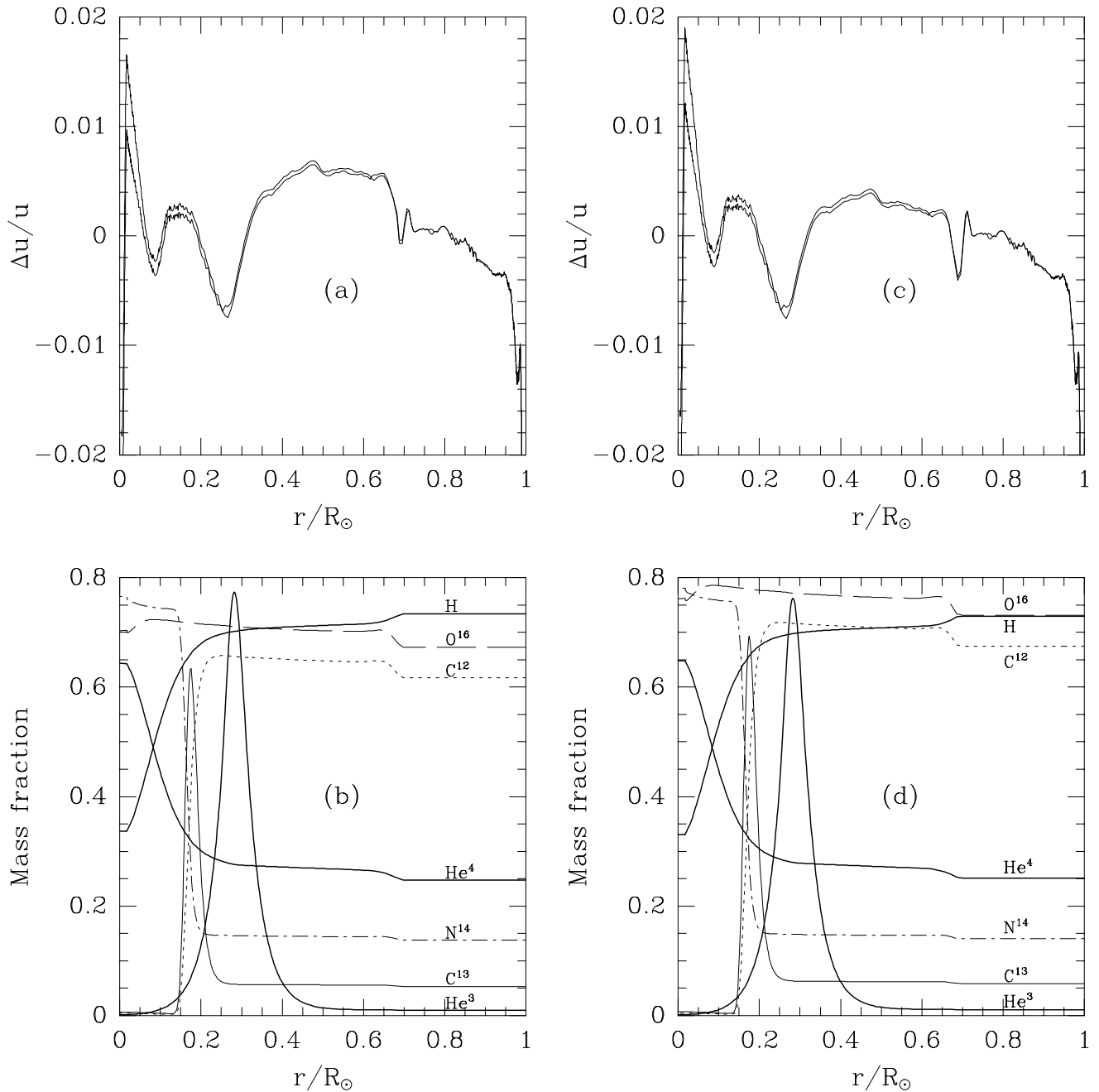


**Fig. 2.** Models with pure element segregation. The presentation is the same as in figure 1. The left graphs represent the model obtained with initial abundances as given by Grevesse (1991) (model 2). The right graphs represent an iterated model computed so that the final abundances are very close to Grevesse’s observed ones (table 4). The  $\Delta u_s$  are clearly smaller for the iterated model. The abundance variations are shown in the bottom graphs. The relative abundance variations in the convective zone compared to the interior (depletion of all the elements except hydrogen) are the same in figures 2b and 2d, but the absolute values differ, so that in fig. 2d the outer values are close to those given in fig. 1b for all elements except helium 4, which is adjusted in the calibration of the model.

**Table 4.** Initial abundances, final surface abundances, and Grevesse mixture in mass fraction.

	Model 2				Model 3			
	Initial mixture used (I2)	Grevesse (1991) with same Y than I2	Final mixture obtained (F2)	Grevesse (1991) with same Y than F2	Initial mixture used (I3)	Grevesse (1991) with same Y than I3	Final mixture obtained (F3)	Grevesse (1991) with same Y than F3
X	0.704800	0.704800	0.734103	0.733309	0.700428	0.701185	0.729746	0.729653
X <sub>He<sup>3</sup></sub>	0.000042	0.000042	0.000040	0.000044	0.000046	0.000042	0.000043	0.000044
Y	0.276200	0.276200	0.247691	0.247691	0.279815	0.279815	0.251347	0.251347
X <sub>C<sup>12</sup></sub>	0.003288	0.003288	0.003084	0.003421	0.003593	0.003271	0.003373	0.003404
X <sub>C<sup>13</sup></sub>	0.000057	0.000057	0.000053	0.000059	0.000063	0.000057	0.000059	0.000059
X <sub>N<sup>14</sup></sub>	0.000976	0.000976	0.000919	0.001015	0.001062	0.000971	0.001001	0.001010
X <sub>N<sup>15</sup></sub>	0.000004	0.000004	0.000004	0.000004	0.000004	0.000004	0.000004	0.000004
X <sub>O<sup>16</sup></sub>	0.009494	0.009494	0.008971	0.009878	0.010313	0.009445	0.009754	0.009828
X <sub>O<sup>17</sup></sub>	0.000007	0.000007	0.000007	0.000007	0.000007	0.000007	0.000007	0.000007
X <sub>O<sup>18</sup></sub>	0.000023	0.000023	0.000022	0.000024	0.000025	0.000023	0.000023	0.000024
X <sub>Ne<sup>20</sup></sub>	0.001603	0.001603	0.001603	0.001668	0.001657	0.001595	0.001657	0.001660
X <sub>Ne<sup>22</sup></sub>	0.000140	0.000140	0.000140	0.000146	0.000145	0.000140	0.000145	0.000145
X <sub>Mg<sup>24</sup></sub>	0.000497	0.000497	0.000497	0.000517	0.000514	0.000494	0.000514	0.000515
X <sub>Mg<sup>25</sup></sub>	0.000068	0.000068	0.000068	0.000071	0.000071	0.000068	0.000071	0.000071
X <sub>Mg<sup>26</sup></sub>	0.000081	0.000081	0.000081	0.000085	0.000084	0.000081	0.000084	0.000084
Z/X	0.026958	0.026958	0.024800	0.025910	0.028207	0.027097	0.025909	0.026040

	Model 4				Model 5			
	Initial mixture used (I2)	Grevesse (1991) with same Y than I2	Final mixture obtained (F2)	Grevesse (1991) with same Y than F2	Initial mixture used (I3)	Grevesse (1991) with same Y than I3	Final mixture obtained (F3)	Grevesse (1991) with same Y than F3
X	0.704016	0.704016	0.725216	0.724734	0.701229	0.701714	0.722576	0.722551
X <sub>He<sup>3</sup></sub>	0.000042	0.000042	0.000076	0.000043	0.000018	0.000042	0.000054	0.000043
Y	0.276984	0.276984	0.256266	0.256266	0.279286	0.279286	0.258449	0.258449
X <sub>C<sup>12</sup></sub>	0.003284	0.003284	0.003149	0.003381	0.003498	0.003273	0.003355	0.003371
X <sub>C<sup>13</sup></sub>	0.000057	0.000057	0.000054	0.000059	0.000062	0.000057	0.000059	0.000059
X <sub>N<sup>14</sup></sub>	0.000975	0.000975	0.000938	0.001003	0.001035	0.000971	0.000996	0.001000
X <sub>N<sup>15</sup></sub>	0.000004	0.000004	0.000004	0.000004	0.000004	0.000004	0.000004	0.000004
X <sub>O<sup>16</sup></sub>	0.009483	0.009483	0.009142	0.009762	0.010052	0.009452	0.009693	0.009733
X <sub>O<sup>17</sup></sub>	0.000007	0.000007	0.000007	0.000007	0.000007	0.000007	0.000007	0.000007
X <sub>O<sup>18</sup></sub>	0.000023	0.000023	0.000022	0.000024	0.000025	0.000023	0.000024	0.000024
X <sub>Ne<sup>20</sup></sub>	0.001602	0.001602	0.001602	0.001649	0.001641	0.001596	0.001641	0.001644
X <sub>Ne<sup>22</sup></sub>	0.000140	0.000140	0.000140	0.000144	0.000144	0.000140	0.000144	0.000144
X <sub>Mg<sup>24</sup></sub>	0.000496	0.000496	0.000496	0.000511	0.000510	0.000495	0.000510	0.000510
X <sub>Mg<sup>25</sup></sub>	0.000068	0.000068	0.000068	0.000070	0.000070	0.000068	0.000070	0.000070
X <sub>Mg<sup>26</sup></sub>	0.000081	0.000081	0.000081	0.000084	0.000084	0.000081	0.000084	0.000083
Z/X	0.026988	0.026988	0.025534	0.026217	0.027787	0.027077	0.026260	0.026296

length. Paquette et al. (1986) proposed a more precise treatment of this problem, with a screened coulomb potential in which the characteristic length is taken as the largest of the Debye length and interionic distance. The Paquette et al. tables of collision integrals have been extensively used in the present paper.

The radiative acceleration on the elements are not included in these computations. From crude approxima-

tions, we suppose that they are negligible in solar type stars (Michaud et al., 1976), but this should be tested in the future, as more precise computations may lead to larger values (Michaud, 1987).

### 2.3. Rotation-induced mixing

We introduced in our computations the rotation-induced mixing as prescribed by Zahn (1992). In a rotating star,

**Table 5.** Predicted neutrino flux in  $10^{10} \text{ cm}^{-2} \cdot \text{s}^{-1}$ .

	$\Phi(\text{pp})$	$\Phi(\text{pep})$	$\Phi(^7\text{Be})$	$\Phi(^8\text{B})$	$\Phi(^{13}\text{N})$	$\Phi(^{15}\text{O})$	$\Phi(^{17}\text{F})$
Model 1	6.00	$1.39 \cdot 10^{-2}$	0.45	$5.45 \cdot 10^{-4}$	$4.52 \cdot 10^{-2}$	$3.85 \cdot 10^{-2}$	$4.90 \cdot 10^{-4}$
Model 2	5.96	$1.39 \cdot 10^{-2}$	0.47	$5.98 \cdot 10^{-4}$	$5.05 \cdot 10^{-2}$	$4.31 \cdot 10^{-2}$	$5.53 \cdot 10^{-4}$
Model 3	5.94	$1.38 \cdot 10^{-2}$	0.48	$6.38 \cdot 10^{-4}$	$5.79 \cdot 10^{-2}$	$4.98 \cdot 10^{-2}$	$6.40 \cdot 10^{-4}$
Model 4	5.96	$1.39 \cdot 10^{-2}$	0.47	$6.06 \cdot 10^{-4}$	$5.09 \cdot 10^{-2}$	$4.35 \cdot 10^{-2}$	$5.60 \cdot 10^{-4}$
Model 5	5.94	$1.38 \cdot 10^{-2}$	0.48	$6.33 \cdot 10^{-4}$	$5.59 \cdot 10^{-2}$	$4.81 \cdot 10^{-2}$	$6.18 \cdot 10^{-4}$

**Table 6.** Predicted neutrino capture rates for the chlorine and gallium experiments in SNU.

Neutrino source	Model 1		Model 2		Model 3		Model 4		Model 5	
	$(\Phi\sigma)_{Cl}$	$(\Phi\sigma)_{Ga}$	$(\Phi\sigma)_{Cl}$	$(\Phi\sigma)_{Ga}$	$(\Phi\sigma)_{Cl}$	$(\Phi\sigma)_{Ga}$	$(\Phi\sigma)_{Cl}$	$(\Phi\sigma)_{Ga}$	$(\Phi\sigma)_{Cl}$	$(\Phi\sigma)_{Ga}$
pp	0	70.722	0	70.353	0	70.042	0	70.303	0	70.068
pep	0.223	2.992	0.223	2.992	0.221	2.965	0.223	2.993	0.221	2.973
$^7\text{Be}$	1.064	32.722	1.117	34.342	1.149	35.352	1.124	34.574	1.146	35.255
$^8\text{B}$	5.781	13.252	6.34	14.534	6.768	15.515	6.42	14.718	6.706	15.372
$^{13}\text{N}$	0.075	2.792	0.084	3.118	0.096	3.576	0.084	3.143	0.093	3.456
$^{15}\text{O}$	0.254	4.46	0.284	4.994	0.329	5.775	0.287	5.045	0.318	5.581
$^{17}\text{F}$	0.003	0.057	0.004	0.065	0.004	0.075	0.004	0.066	0.004	0.072
Total	7.4	126.997	8.052	130.398	8.567	133.3	8.142	130.842	8.488	132.769

due to centrifugal effects, the gravity equipotentials are no more spherical, which induces a circulation of matter between polar and equatorial regions: the so-called meridional circulation. This circulation itself induces a transport of angular momentum, thereby creating shears which become unstable in the horizontal direction, while the vertical shears are stabilized by the density gradient. This large scale horizontal turbulence decays into small scales and becomes 3D when the turnover rate of the turbulence exceeds the angular velocity.

Meanwhile the horizontal turbulence “cuts down” the effect of advection on the transport of the chemical species, as the elements which go up in the upward flow of matter can be transported into the downward flow by horizontal motions before reaching the top layers. The transport of angular momentum is more efficient than the transport of chemicals. In the limit of extremely large horizontal diffusivity, the chemical composition is constant along a level surface, and the transport of chemicals is negligible. The angular momentum behaves differently as, when the rotation velocity is constant along a level surface, the angular momentum is not, so that it is still transported.

The horizontal transport of angular momentum smoothes out the original meridional circulation. Taking this feedback effect into account, Zahn (1992) showed that the whole process is stopped within an Eddington-Sweet time-scale, unless angular momentum is extracted from the star due to a wind.

In case of a moderate wind which extracts angular momentum at the rate  $(\frac{dJ}{dt})$ , an asymptotic regime is reached with a circulation velocity as a function of radius given by

(following Zahn (1992) eq.4.15):

$$U(r) = \frac{5}{\rho(r) r^4 \Omega} \frac{3}{8\pi} \left( \frac{dJ}{dt} \right) \quad (1)$$

where  $\rho$  is the local density, or:

$$U(r) = \frac{5}{2} \frac{1}{\Omega(r) r M(r)} \frac{\rho_m}{\rho(r)} \left( \frac{dJ}{dt} \right) \quad (2)$$

where  $\Omega(r)$  is the local angular velocity,  $M(r)$  the mass inside radius  $r$  and  $\rho_m$  the average density inside radius  $r$ .

The effective diffusion coefficient is then expressed by Zahn’s eq. 4.21 :

$$D_{eff} = \frac{C_h}{50} \frac{r|U(r)|}{\alpha} \quad (3)$$

where  $C_h$  is a parameter related to the horizontal viscosity ( $C_h \lesssim 1$ ) and  $\alpha$  is related to the differential rotation:

$$\alpha = \frac{1}{2} \frac{d \ln(r^2 \Omega)}{d \ln r} \quad (4)$$

If the deviation of  $\Omega$  from solid rotation is neglected ( $\alpha = 1$ ), and if  $\Omega$  is supposed to decrease with time following a “Skumanich law” for which  $\Omega \propto t^{-\frac{1}{2}}$  we obtain:

$$\frac{dJ}{dt} \propto \Omega^3 \quad (5)$$

and the effective mixing coefficient is of the form:

$$D_{eff} \simeq r \cdot U(r) \propto \frac{\Omega^2}{\rho r^3} \quad (6)$$

Equation (3) has been used in the present computations with  $\alpha = 1$ . The proportionality factor  $C_h$  has been adjusted to obtain the right lithium depletion in the Sun (section 4).

#### 2.4. Stabilizing $\mu$ -gradients

Mixing processes in stars may be stabilized in the regions where the mean molecular weight rapidly decreases with increasing radius. This occurs specially in the nuclear burning core: we can thus infer that the rotation-induced mixing becomes inefficient as soon as the  $\mu$ -gradient becomes larger than some critical value. This question has been discussed by several authors (Mestel (1965), Huppert and Spiegel (1977)). Although no precise value can be given for this critical  $\mu$ -gradient, an order of magnitude can be obtained from simple considerations.

Huppert and Spiegel (1977) suggest that mixing can penetrate the nuclear burning core within a scale height given by:

$$h \simeq r \frac{\Omega(r)}{N_\mu} \quad (7)$$

where  $r$  is the local radius,  $\Omega(r)$  the angular rotation velocity and  $N_\mu$  the buoyancy frequency due to the  $\mu$ -gradient.

$$N_\mu^2 \simeq \frac{GM(r)}{r^2} \left| \frac{d \ln \mu}{dr} \right| \quad (8)$$

From eq. (7) we can derive a critical  $\mu$ -gradient obtained by specifying that  $h$  must be a small fraction of  $r$  ( $h = \varepsilon r$ ):

$$(\nabla \ln \mu)_c \simeq \frac{1}{\varepsilon^2} \frac{r_c^2 \Omega^2(r_c)}{GM(r_c)} \quad (9)$$

where all the quantities should be computed at the place where the actual  $\nabla \ln \mu$  is equal to the critical one.

With values of  $r_c$  between  $0.1 R_\odot$  and  $0.2 R_\odot$  and values of  $\Omega$  between  $3 \times 10^{-6}$  ( $V_{R_\odot} \simeq 2 \text{ km.s}^{-1}$ ) and  $10^{-4}$  ( $V_{R_\odot} \simeq 70 \text{ km.s}^{-1}$ ) we find, for  $\varepsilon = 0.1$ :

$$4 \times 10^{-15} < (\nabla \ln \mu)_c < 4 \times 10^{-12}$$

Solar structure computations lead to stronger constraints on the critical  $\mu$ -gradient. With  $(\nabla \ln \mu)_c \lesssim 10^{-14}$  no mixing could occur in the Sun after 0.1 Gyr. With  $(\nabla \ln \mu)_c \gtrsim 10^{-12}$  too much mixing would occur in the core, and the consistency with helioseismology would be lost (Gaigé 1994). Our best model is obtained with  $(\nabla \ln \mu)_c = 4 \times 10^{-13}$  (section 4.3).

#### 2.5. The diffusion routine

The stellar evolution code used in these computations is the Geneva code, described several times in the literature. The system of nuclear reactions and the abundance variations in the standard models are computed as in Maeder (1983). They are separately determined for 15 isotopes: H,  $^3\text{He}$ ,  $^4\text{He}$ ,  $^{12}\text{C}$ ,  $^{13}\text{C}$ ,  $^{14}\text{N}$ ,  $^{15}\text{N}$ ,  $^{16}\text{O}$ ,  $^{17}\text{O}$ ,  $^{18}\text{O}$ ,  $^{20}\text{Ne}$ ,  $^{22}\text{Ne}$ ,

$^{24}\text{Mg}$ ,  $^{25}\text{Mg}$ ,  $^{26}\text{Mg}$ . The heavier elements are combined in a single mass fraction Z.

We have added in this code a diffusion routine for each isotope in a similar way as described in CVZ. The diffusion equations are written in lagrangian coordinates as :

$$\frac{\partial c_i}{\partial t} = D_i \frac{\partial^2 c_i}{\partial m^2} + E_i \frac{\partial c_i}{\partial m^2} + F_i c_i \quad (10)$$

where  $c_i$  stands for the concentration of isotope  $i$ , and:

$$\begin{aligned} D_i &= (4\pi r^2 \rho)^2 (D_{eff} + D_s^i) \\ E_i &= (4\pi r^2 \rho)^2 \left( 4\pi \frac{\partial r^2 \rho (D_{eff} D_s^i)}{\partial m} - V_i \right) \\ F_i &= -\lambda_i - 4\pi \frac{\partial (r^2 \rho V_i)}{\partial m} \end{aligned} \quad (11)$$

Here  $D_{eff}$  is the effective mixing coefficient (the same for all the isotopes) while  $D_s^i$  is the segregation coefficient, computed for each isotope using Paquette et al. (1986) tables.  $V_i$  represents the segregation (microscopic) velocity. The nuclear destruction rate  $\lambda_i$  is only included in  $F_i$  for lithium and beryllium, which are treated separately from the network.

For the 15 isotopes included in the nuclear network, the computation procedure is the following:

- at each evolutionary step, equation (10) is solved separately for all the isotopes except hydrogen. The method is the same as described in CVZ: a Cranck-Nicholson scheme with the inversion of a tridiagonal matrix including all the mesh points down to the center
- this diffusion routine is used with a smaller time step as the evolution time step, for a better precision. Typically 20 resolutions of the diffusion equation are done between two computations of a complete model
- the new mass fractions of each isotope are computed, taking into account the normalisation equation:

$$X_1 + \sum_{k \neq 1} X_k + Z = 1$$

Satisfying this equation needs a consistent resolution of the abundances of all the considered isotopes with the inversion of a  $(k + 1)$  order matrix

- the abundance variations due to the nuclear reactions are then computed.

### 3. Helioseismological constraints

We shall compare the  $u(r) = \frac{P(r)}{\rho(r)}$  function and the  $Y_{surf}$  quantity in our theoretical models with those in the seismic model derived from the observed p-mode frequencies with the method described by Dziembowski et al. (1994). The seismic model that we adopt here differs from the one presented in that paper in two respects. First we use new frequency data for  $\ell \leq 3$  degrees from BISON network (Elsworth et al., 1994). This has a most noticeable effect in  $u(r)$  in the core. The second is the use of OPAL rather than MHD equation of state (EOS) in the reference model



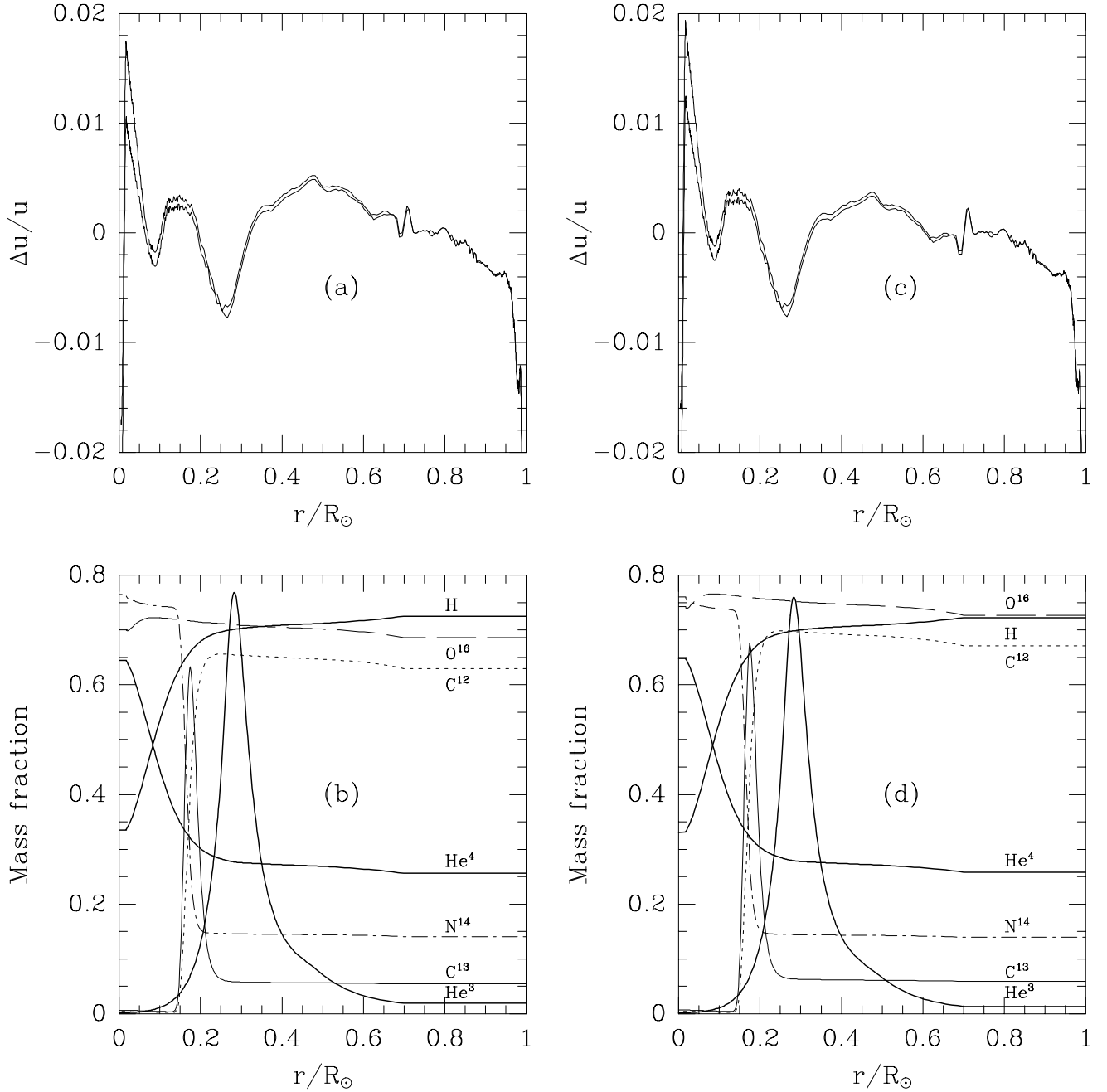


**Fig. 3.** Models with element segregation and rotation-induced mixing. The presentation is the same as in figures 1 and 2. The left graphs correspond to models computed with initial Grevesse (1991) abundances (model 4). The right graphs correspond to iterated models so that the final abundances are close to the observed Grevesse (1991) abundances (model 5). Here the parametrisation of the rotation-induced mixing is that proposed by Zahn (1992) in the asymptotic regime. The mixing efficiency is supposed annihilated when the  $\mu$ -gradient is larger than  $4 \times 10^{-13} \text{ cm}^{-1}$  (see text). This cut-off is very important as a deeper mixing inside the nuclear burning core destroys the consistency of the computed and observed  $u$  values. Here the  $\Delta u$  values are slightly smaller in figures 3a and 3c than in figures 2a and 2c. Meanwhile lithium and beryllium are destroyed as observed in the Sun (see figure 4).

adopted for the inversion (for consistency with the opacities), which does not change the  $u$  values in a significant way. The only important consequence of this change is a somewhat higher seismic value for  $Y_{surf}$ .

Within the adiabatic part of the convective zone the sound speed is determined solely by the value of the  $M$  to  $R$  ratio and by the value of adiabatic exponent,  $\Gamma_1$ . Comparison of the model and the seismic  $u(r)$  in this region provides therefore a test of the EOS. The situation in the radiative interior is more complicated. Let us note that approximately  $u \propto \frac{T}{\mu}$ , and therefore the radiative transport of energy and the element diffusion directly affect  $u(r)$  below the convective envelope.

In general, it is not possible to disentangle the uncertainty in the opacity and in the diffusion coefficients. Only the convective overshooting leading to a discontinuity in  $\frac{du}{dr}$  leaves a signature in the sound speed which is seismically detectable. Monteiro et al. (1994) looked for it and came up with an upper limit on the extent of such overshooting, which is 0.07 of the local pressure distance scale or  $0.006 R_\odot$ . In our models such overshooting has been ignored and the above results show that this is a good approximation. The bottom of the convective zone in such case may be determined quite accurately. In the seismic model used in this work  $r_{cz} = (0.7137 \pm 0.0002) R_\odot$ , which agrees very well with the first accurate helioseismic value  $r_{cz} = (0.713 \pm 0.003) R_\odot$  (Christensen-Dalsgaard et al., 1993).

There are still some uncertainties due to the opacities. Unfortunately, we do not have a good way to assess limits for the induced modifications. Alternative opacities (OP, Seaton et al. 1994) are by about 40 percent lower at temperature and density ranges of interest here. However, this large difference may perhaps be due to a neglect of the plasma effects on the atomic properties, in the OP calculations, and therefore may not serve as an estimate of the uncertainty.

In such a situation it is important to make use of the additional constraint which is the value of  $Y_{surf}$  determined by means of helioseismology. In this comparison the uncertainty in the opacity data is rather unimportant. The possibility of a seismic measure of helium abundance rests on a large value of the  $\Gamma_1$  derivative with respect to  $Y$  in the HeII ionization zone and obviously requires very accurate thermodynamical data. The seismic values obtained with Dziembowski et al. (1994) method of inversion for two versions of the EOS adopted in the reference model are

$$Y_{surf} = 0.2440 \pm 0.0003 \text{ for MHD}$$

$$Y_{surf} = 0.2505 \pm 0.0003 \text{ for OPAL}$$

The test of  $\Gamma_1$  in the lower convective zone points to OPAL data as more accurate, which should be expected as the OPAL EOS is obtained in a more fundamental way. We stress that the model values of  $Y_{surf}$  is quite insensitive to the choice of the EOS. The errors given above reflect only the frequency errors quoted by

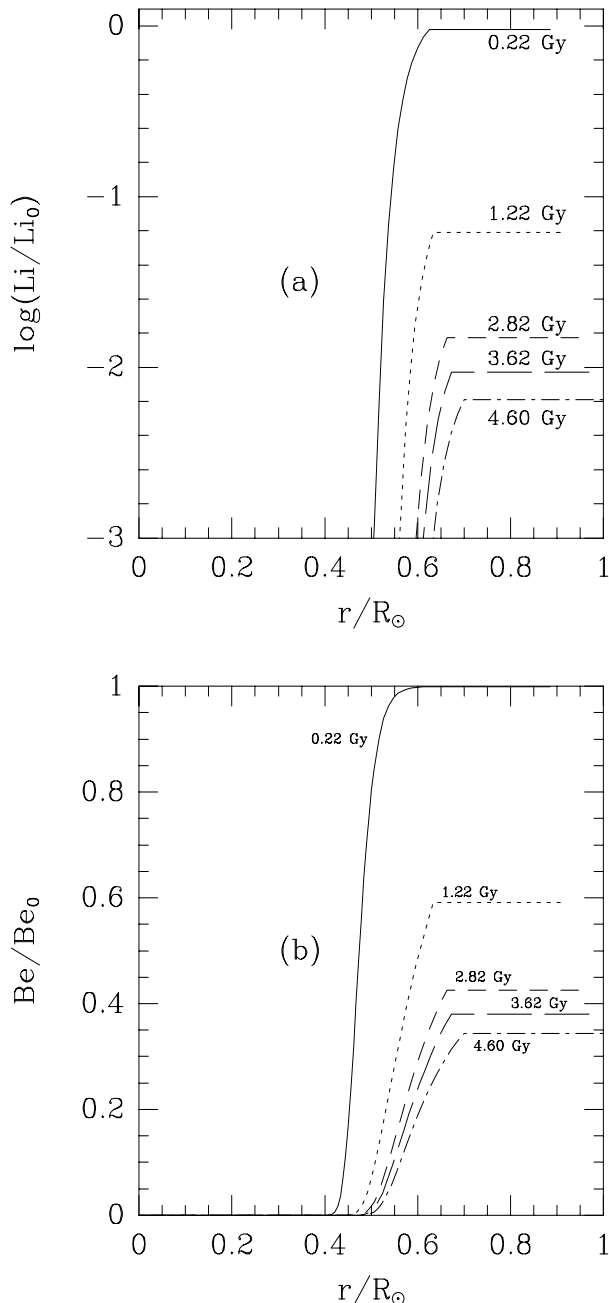


**Fig. 4.** Lithium (top) and beryllium (bottom) variations profiles in the best model 5 as a function of age. At the age of the Sun lithium is destroyed by 155 and beryllium by 2.9.

the observers. The actual uncertainty in the seismic values is much larger. For instance, Basu and Antia (1995) find 0.246 and 0.249 for the corresponding quantities. The results are indeed depended on the adopted method of inversion. In particular they depend on smoothing the  $\frac{\Delta u}{u}$  function which describes the relative differences between the solar and the model  $u(r)$ . Without smoothing, which is perhaps a better choice is the only goal is the determination of the He abundance, our method yields  $Y_{surf} = 0.2548$  for the OPAL EOS. (Pamyatnykh, private communication). The problem certainly requires further examination because, as we shall see, it is essential to reduce the uncertainty to the  $10^{-3}$  level.

#### 4. The results

Five solar models have been computed and compared to the helioseismological sun (Figures 1 to 3). The values of the characteristic parameters of the models, abundances and neutrino production are given in tables 2 to 6.

##### 4.1. The “standard” model

This model includes the physics as discussed in section 2-1, with no element segregation and no other mixing than inside the convection zone. The comparison with helioseismology is presented in figure 1a, and the fractional abundance of several interesting elements in figure 1b. The two curves in figure 1a correspond to the uncertainty in the helioseismological inversion.

A comparison of seismic values of  $r_{cz}$  and  $Y_{surf}$  with those for Model 1, given in Tables 2 and 3 reveals large differences. Also large differences are seen in the sound speed behavior throughout the whole interior as seen in Fig. 1. We do not pay attention to the differences in the outer part of the convective zone. They may be accounted for by inadequacies of the mixing length theory (outermost part) and in the MHD equation of state. Our main concern is the value  $\frac{\Delta u}{u}$  of about 0.015 in the outer part of the radiative interior, which is too large.

Of course lithium is not depleted in model 1, neither is beryllium, and the solar neutrino fluxes are too high compared with the results of the solar neutrino detectors (tables 5 and 6).

##### 4.2. Models with pure element segregation (no mixing)

– the first of these models (model 2) has been obtained with element segregation of helium and the initial abundances as given by Grevesse (1991).

We see at once, from figure 2a, that the discrepancy below the convective zone is considerably reduced compared to model 1, while figure 2b shows the influence of segregation on the fractional abundances of the elements. The basic reason for the improvement in the  $u$  value is due to helium diffusion, which leads to a diminution of the helium abundance of about 10% inside the convection zone

and below, thereby decreasing the local mean molecular weight.

– model 2 is however inconsistent with the observed present element abundances due to the segregation. Model 3 is similar to model 2, but iterated so that the final abundances correspond to the values given by Grevesse (1991). Table 4 shows the final abundances obtained, compared to the observations. It is also interesting to compare figure 2d with figure 2b to see the difference in the fractional abundances of the elements.

There is a dramatic improvement in the agreement with the seismic model once the element segregation is introduced. In Model 3 the coincidence of  $r_{cz}$  and  $Y_{surf}$  with the seismic values is so perfect that, admittedly, it may be to some extent coincidental.

From tables 2 to 6 we check that models 2 and 3 are well calibrated, while the neutrino fluxes are not decreased, as expected.

We insist on the fact that these models are computed without any arbitrary parameters: element segregation is a simple consequence of the stellar physics, with no special assumption added. They should not be considered as non-standard models, but as improved standard solar models.

Lithium and beryllium are not more depleted than helium in these models, as the depletion is only due to element segregation. It is necessary to introduce a mild mixing below the convection zone to account for the observed abundances of these elements.

##### 4.3. Models with element segregation and rotation-induced mixing

Rotation-induced mixing as described in section 2 have been added in the computations of models 4 and 5. Here a parameter has been adjusted (namely the  $C_h$  factor in Zahn’s prescription) so as to obtain a lithium depletion as observed. In consequence these two models must be considered as non-standard.

In both models the mixing coefficient has been cut off at the core for a  $\mu$ -gradient of  $4 \times 10^{-13}$ . Models with mixing down to the solar core lead to large discrepancies with helioseismology. On the other hand, in our models, the mixing is inefficient in the region of energy production in the Sun, and the consistency with helioseismology is even better than for models without mixing (see figures 3a and 3c).

Model 4 is obtained with initial abundances as in Grevesse (1991), while model 5 has been iterated so that the final abundances are those of Grevesse (1991) (see table 4). It is interesting to note that model 5 is still closer to the helioseismological Sun than model 4: in all cases improving the physics leads to better results compared to the observations, which is very encouraging.

While an inclusion of the element mixing somewhat improves the agreement in the  $u(r)$ , it slightly destroys the perfect coincidence in  $r_{cz}$  and  $Y_{surf}$ . We do not con-

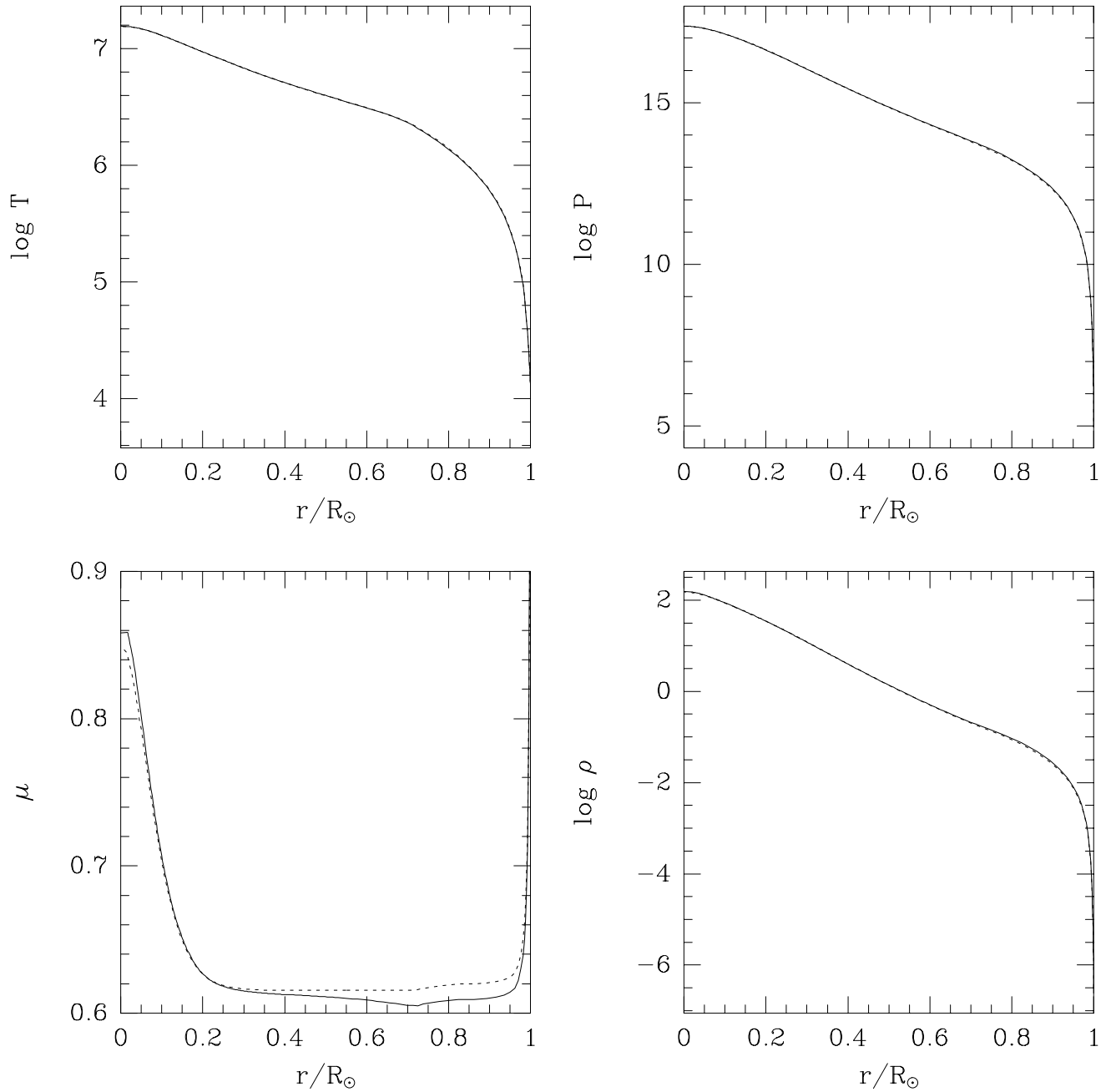


**Fig. 5.** Comparison between the parameters  $\log T$ ,  $\log P$ ,  $\mu$  and  $\log \rho$  in our “best model” 5 (solid lines) and the standard model (dashed lines). While no clear difference can be seen at these scales for  $T$ ,  $P$  and  $\rho$ , the difference in  $\mu$  due to the element segregation is clearly visible. It is the basic reason for the better agreement of this model with the helioseismological sound speed, compared to the standard model.

sider any of these differences as really significant. Let us note that the seismic value of  $Y_{surf}$  obtained without regularization, which we regard as more credible, is right in the middle of the values for model 3 and 5. The difference between the two models is 0.005. An accuracy of 0.001 in seismic  $Y_{surf}$  would thus yield an interesting constraint on the element mixing. The data certainly allow such accuracy. The problems lie in data analysis and in reliability of the EOS.

In model 5 lithium is depleted with a ratio 1/155 and beryllium with a ratio 1/2.9, which is very close to the observations. The lithium and beryllium abundance profiles for various times are given in figure 4.

The difference in  $\mu$ -values from models 1 and 5 is given in figure 5.

## 5. Conclusion

Model 5 is presently our best model. It is a well calibrated model, including element segregation and a parametrized rotation-induced mixing. It leads to a very good fit between the computed  $u = \frac{P}{\rho}$  function and that deduced from helioseismology below the solar convection zone. The consistency is also very good inside the convection zone except at the surface where a better mixing treatment should be introduced. Lithium and beryllium are depleted as observed. The neutrino fluxes remain too high.

Below a radius of 0.4 of the solar radius a discrepancy remains in the  $u$  curves. Although the uncertainty on  $u$  is much larger in the core than at the surface, these features seem significant. This specific problem will be addressed in a forthcoming paper.

Element segregation certainly takes place in the Sun's interior. It involves no nonstandard physics and its occurrence is fully confirmed by the results of helioseismic inversion. On the other hand the macroscopic mixing is a hypothetical effect which provides a natural explanation of the Li and Be deficit but demands convincing observational confirmations and constraints. At present stage we may only conclude that there is no conflict between models reproducing solar Li and Be abundances and helioseismic data. There are good prospects for obtaining stringent constraints on the hypothetical mixing processes from helioseismology. On the road to this goal we regard as most important to improve reliability and accuracy of the He abundance determination. Progress should also be made in assessing uncertainties in the opacity data, so that the information about the sound speed behavior may lead to a more direct probe of the He distribution in the outer part of the radiative interior.

*Note:* Model 5 is available on request by electronic mail at the address: richard@obs-mip.fr.

*Acknowledgements.* We thank Alosha Pamyatnykh for his collaboration on the new version of the seismic model and for a

helpful discussion. The work was supported, in part, by PICS "France-Pologne".

## References

- Alecian, G., Vauclair, S., 1981, A&A 101, 16  
 Bahcall, J.N., Loeb, A., 1990, ApJ 360,267  
 Bahcall, J.N., Pinsonneault, M.H., 1992, *Reviews of Modern Physics* 64,885  
 Basu, S. and Antia, H.M., 1995 in *Proceedings of 4th SOHO Workshop: Helioseismology*, ESA SP 376, ESTEC, Noordwijk, eds, J.T. Hochsma, V. Domingo, B. Fleck  
 Burgers, J.M., 1969 *Flow Equations for Composite Gases*, New York: Academic Press  
 Caughlan G.R., Fowler W.A., 1988, *Atomic Data Nuc. Data Tables* 40, 283  
 Chapman, S., 1917, MNRAS 77,540  
 Chapman, S., Cowling, T.G., 1970, *The Mathematical Theory of Non-Uniform Gases*, Cambridge University Press, 3rd ed.  
 Charbonnel, C., Vauclair, S., Zahn, J.P. 1992, A&A 255, 191 (CVZ)  
 Charbonnel, C., Vauclair, S., Maeder, A., Meynet, G., Schaller, G. 1994, A&A 283, 155  
 Christensen-Dalsgaard J., Däppen W., Lebreton Y., 1988, *Nat.*, 336, 634  
 Christensen-Dalsgaard, J., Proffitt, C.R., and Thompson, M.J., 1993, ApJL, 403, L75  
 Cox, A.N., Guzik, J.A., Kidman, R.B. 1989, ApJ 342, 1187  
 Däppen W., Mihalas D., Hummer D.G, Mihalas B.W., 1988, ApJ 332, 261  
 Demarque P., Guenther D.B., 1991 in *Solar Interior and Atmosphere* A.N. Cox, W.C. Livingston, M.S. Matthews ed., The University of Arizona Press, p. 1186  
 Dziembowski, W.Q., Goode, P.R., Pamyatnikh, A.A., Sienkiewicz, R., 1994, ApJ 432, 417  
 Eddington, A.S., 1916, MNRAS 77, 16  
 Eddington, A.S., 1926, *The Internal Constitution of Stars*, Dover Pub.  
 Elsworth, Y., Howe, R., Isaak, G.R., McLeod, C.P., New, R. 1994, ApJ, 434, 801  
 Gaigé, Y., 1994, Thesis, Université Paul Sabatier, Toulouse  
 Graboske H.C., de Witt H.E., Grossman A.S., Cooper M.S., 1973, ApJ 181, 457  
 Grevesse, N., 1991, A&A 242, 488  
 Guenther D.B., 1989, ApJ 339, 1156  
 Hummer D.G, Mihalas D., 1988, ApJ 331,794  
 Huppert, H.E., Spiegel, E.A., 1977, ApJ 213, 157  
 Iglesias C.A., Rogers F.J., Wilson B.G., 1992, ApJ 397, 717  
 Kurucz R.L., 1991, in *Stellar Atmospheres: Beyond Classical Models*, NATO ASI Series C, Vol. 341, Eds. L.Crivellari, I.Hubeny, D.G.Hummer  
 Maeder, A. 1983, A&A 120, 113  
 Mestel, L., 1965, *Stellar Structure*, in *Stars and Stellar Systems* vol. 8 (ed. G.P. Kuiper, B.M. Middlehurst; Univ. Chicago Press), 465  
 Michaud, G., 1970, ApJ 160, 641  
 Michaud, G., 1987, *Physica Scripta* 36, 112  
 Michaud, G., Charland, Y., Vauclair, S., Vauclair, G., 1976, ApJ 210, 447

- Michaud, G., Vauclair, S., 1991, in *Solar Interior and Atmosphere* A.N. Cox, W.C. Livingston, M.S. Matthews ed., The University of Arizona Press, p. 304
- Mihalas D., Hummer D.G., Däppen W., 1988, ApJ 331, 815
- Monteiro, M.J.P.F.G., Christensen-Dalsgaard, J., and Thompson, M.J., 19.. A&A, 283, 247
- Montmerle, T., Michaud, G., 1976, ApJS 31, 489
- Paquette, C., Pelletier, C., Fontaine, G., Michaud, G., 1986, ApJS 61, 177
- Proffitt, C.R., 1994, ApJ 425, 849
- Proffitt, C.R., Michaud, G., 1991, ApJ 380, 238
- Proffitt, C.R., VandenBerg, D.A., 1991, ApJS 77, 473
- Seaton, M.J., Yu Yan, Mihalas, D. and Pradhan, A.K., 1994, MNRAS, 266, 805
- Richer, J., Michaud, G., 1993, ApJ 416, 312
- Schatzman, E., 1945, *Ann. d'Astr.* 8,143
- Thoul, A.A., Bahcall, J.N., Loeb, A., 1994, ApJ 421, 828
- Turck-Chieze, S., Lopes, I. 1993, ApJ 408, 347
- Vauclair, S., Hardorp, J., Peterson, D.M. 1991, ApJ 227, 526
- Vauclair, S., Vauclair, G., 1982, ARA&A 20, 37
- Zahn J.P., 1992, A&A 265, 115